Proc. Indian Acad. Sci. (Chem. Sci.), Vol. 95, Nos 1 & 2, July 1985, pp. 141–157.

Ligand hyperfine and exchange interactions in a low-spin d^7 system

E BALASIVASUBRAMANIAN and P T MANOHARAN
Department of Chemistry, Indian Institute of Technology, Madras 600036, India.

Abstract. The single crystal EPR results of $[NiBr_2(diars)_2]Br$, a low spin Ni(III) complex, magnetically diluted in $[Co(NO)Br(diars)_2]Br$ show a very large bromine hyperfine coupling. The experimental g, ligand hyperfine splitting due to arsenic and bromine and spin densities are compared with other analogous diphos and diars complexes. The unpaired electron is essentially in the d_{z^2} orbital and there is extensive delocalization over all the ligand nuclei due to extended 4*s* and 4*p* radial wave functions. On the other hand the pure crystal of $[NiBr_2(diars)_2]Br$ shows single exchange averaged EPR line. Linewidth analysis using the existing theories of exchange gives values of roughly 800 G and 380 G for respectively isotropic and intersite exchange interactions in this system.

Keywords. Nickel diarsine complex; electron paramagnetic resonance; hyperfine splitting; exchange interactions; intersite exchange.

1. Introduction

Considerable single crystal EPR data on the six-coordinated low spin d^7 Ni(III) complexes of ligands *o*-phenylenebisdimethylphosphine(diphos) and *o*-phenylenebisdimethylarsine(diars) are available in literature (Kreisman *et al* 1968; Manoharan and Rogers 1970; Bernstein and Gray 1972; Sethulakshmi *et al* 1979; Balasivasubramanian *et al* 1982). The four important systems under consideration are $NiX_2(diphos)_2^+$ and $NiX_2(diars)_2^+$ where X is chlorine and or bromine. Of the four species, detailed single crystal EPR studies on three of them have already been reported (Bernstein and Gray 1972; Sethulakshmi *et al* 1979; Balasivasubramanian *et al* 1982). The only species left out in this series is $NiBr_2(diars)_2^+$. The intention of our study on this system is to make a good comparison between the dihalo complexes containing two different bidentate ligands *viz* diphos and diars. A general conclusion based on the single crystal EPR studies on all systems other than $NiBr_2(diars)_2^+$ reveals that the delocalization of the molecular wavefunction for the unpaired electron of this complex should be most pronounced. This might lead to an enhanced hyperfine interaction with the ligand nuclei. Further it was thought that the effect of this enhanced hyperfine broadening on the shape and width of the single crystal EPR resonance absorption of the pure (undiluted) compound would be very interesting to investigate. In this paper we report the EPR study of $[NiBr_2(diars)_2]^+Br^-$ diluted in an isomorphous diamagnetic host lattice $[Co(NO)Br(diars)_2]Br$; also, we have made an attempt, in the light of the available theories, to understand the nature and magnitude of the various cooperative magnetic interactions present in the pure solid.

2. Experimental

The trans-dibromobis[*o*-phenylenebisdimethylarsine] nickel(III) bromide $[NiBr_2(diars)_2]Br$ was prepared according to the procedure of Nyholm (1950). The

trans-bromonitrosylbis[*o*-phenylenebisdimethylarsine] cobalt(III)] bromide was made following the method of Feltham and Nyholm (1965). Single crystals suitable for EPR measurements were grown by slow evaporation of an alcoholic solution of the cobalt(III) complex containing 1 mol% of nickel(III) complex. Small reddish brown, diamond-shaped crystals of pure $[NiBr_2(diars)_2]Br$ were grown from nitromethane solution.

EPR measurements were made at *X*- and *Q*-band frequencies at 300 K using Varian E-112 spectrometer with 100 kHz modulation coils. DPPH was used as a *g*-calibrant. All linewidths reported here are peak-to-peak width of the first derivative spectrum ΔB_{pp}. The error in the linewidth measurements is ± 2 G. However, in the case of diluted crystals it was noticed that nickel(III) has not gone in with adequate concentration in the cobalt(III) lattice. As a result of this poor concentration of Ni(III) in the small crystals of Co(III) complex, the *X*-band spectrum was extremely noisy. Furthermore, the complicated EPR spectra from two different sites with a large number of ligand superhyperfine structure made it almost impossible to make a good analysis of the *X*-band EPR spectral data. Hence all the single crystal EPR measurements on this system were made on the *Q*-band spectrometer.

3. Results and discussion

3.1 EPR *of* $[NiBr_2(diars)_2]Br$ *diluted in* $[Co(NO)Br(diars)_2]Br$

3.1a *Crystal structure of* $[Fe(NO)Br(diars)_2]ClO_4$: The diamagnetic host lattice chosen for this study viz $[Co(NO)Br(diars)_2]Br$ is isomorphous to $[Fe(NO)Br(diars)_2]ClO_4$. The crystal structure of this iron(III) complex has been received by us by a private communication from Professor Dahl. The unit cell is tetragonal with space group $P4/n(C_{4h}^3)$. The lattice parameters are: $a = 17{\cdot}11 \pm 0{\cdot}03$ Å, $c = 9{\cdot}94 \pm 0.02$ Å, $Z = 4$. The cation $Fe(NO)Br(diars)_2^+$ is situated in the centre of symmetry. The cation has approximately C_{2v} symmetry, the unique axis being Br–Fe–NO. The projection down the *c* axis is shown in figure 1. The phenylene rings are not coplanar with the $FeAs_4$ plane, but are inclined. The dihedral angle between the normals to a phenylene ring and $FeAs_4$ plane was found to be 9° in the iron(III) complex $[Fe(NO)Br(diars)_2]ClO_4$. The average nonbonding Br. . . . CH_3 distance of 3·61 Å is much shorter than the sum of the corresponding van der Waals radii (3·95 Å). Similar distortions do occur in the case of other diars complexes of iron and hence it is possible that such distortions might also occur in the cobalt complex. Silverthorn and Feltham (1967) suggested a nonlinear Fe–N–O bond axis on the basis of their studies on the electronic and infrared spectra. The situation in the cobalt(III) complex cannot be much different from the iron(III) complex because of the isomorphous character. From EPR point of view, there will be two magnetically inequivalent sites when Ni(III) is introduced into the diamagnetic Co(III) lattice. As a result, two sets of Br–Co–NO hence Br–Ni–Br axes will be present which will be mutually perpendicular to each other, one approximately along the *a*- and the other along the *b*-axes.

3.1b *g-tensor*: Though the measurements were done on the three orthogonal planes, 100, 010 and 001, the first two yielded identical spectral data and the angular variation of *g* and *A* tensors in these two planes are quite similar. This is made possible because of the tetragonal cell. When the magnetic field is in the first two planes and when the field is

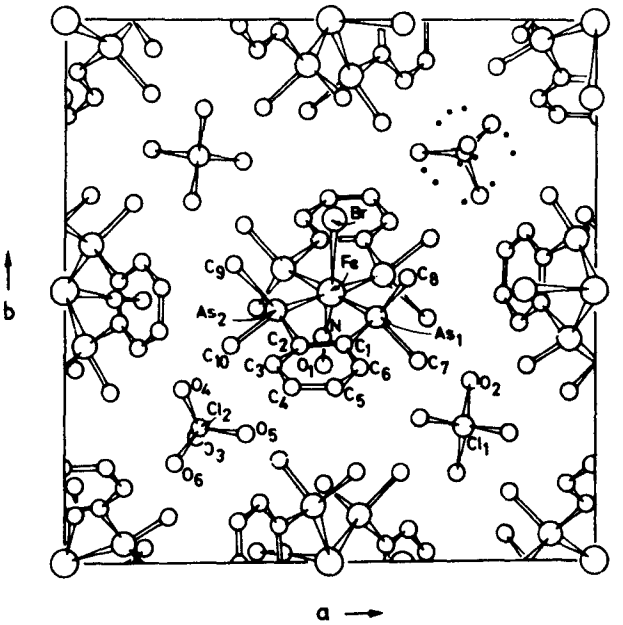

Figure 1. The projection of $[Fe(NO)Br(diars)_2]^+$ down the c axis.

parallel either to the a or the b axis, half of the molecules are roughly aligned parallel to the NO–Co–Br axis and hence the Br–Ni–Br axis of the dopant molecule. The remaining half of the molecules will have the bisector of the diars ligand ring parallel to the applied field. Hence the EPR spectrum in such a case is made up of one set of multiplets due to the $g_{\|}$ and another set of multiplets due to $g_{\perp}$ as shown in figure 2.

The first set of molecules changes on rotation from $g_{\|}$ to $g_{\perp}$ and back again to $g_{\|}$ during a 180° rotation. However, the g-value of the other set does not change much due to the very small changes in the g-values of the equatorial plane containing the four arsenic atoms. This is quite obvious from figures 3a and 3b.

When c-axis is the rotation axis both sets of molecules move from roughly a $g_{\|}$ direction to $g_{\perp}$ direction. It is to be noted that the $g_{\|}$ and $g_{\perp}$ sets of lines contain hyperfine splitting due to two Br's and four As's and hence there is considerable overlap between the spectra due to two inequivalent sites except where the g-values have considerable difference. This has led to some complication in identifying the exact position of the g-values. Hence the fitting was done only with the points which we could surely identify.

A least-squares fitting of the g-values was done assuming the direction cosines obtained from crystallographic data given in table 1. There is remarkable similarity between the experimental and calculated points using Br–Ni–Br as the unique axis corresponding to $g_{\|}$. The g-anisotropy in the equatorial plane, however minimum, could be identified by this fit. The g-values thus obtained are also given in table 1.

3.1c *Ligand hyperfine interaction from* ^{75}As *and* ^{79,81}Br: Since the EPR measurements were made using naturally abundant isotopes of Ni, no metal hyperfine splitting due to ^{61}Ni($I = 3/2$ with natural abundance of 1·19%) is expected to be clear enough for

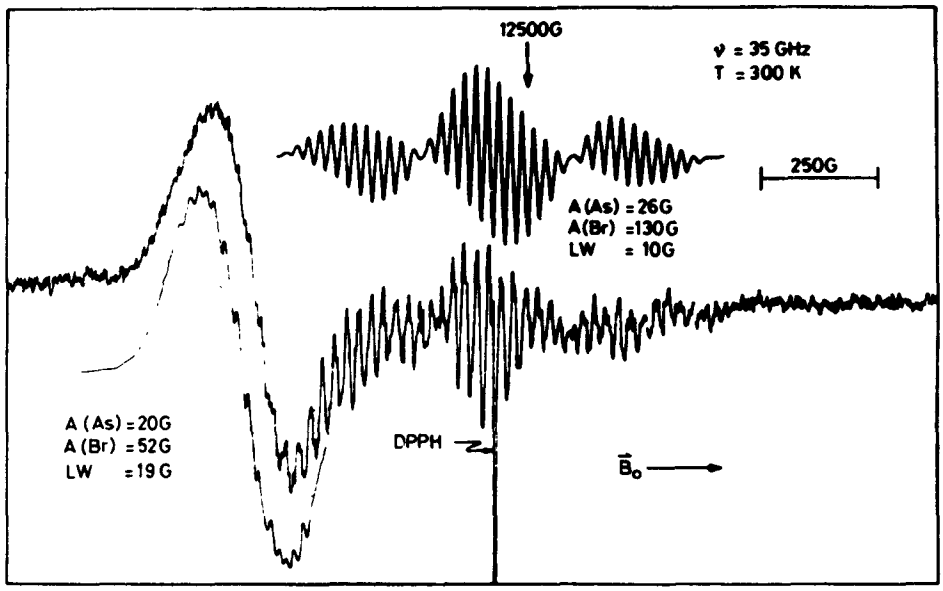

Figure 2. Experimental and simulated single crystal EPR spectra of $[NiBr_2(diars)_2]^+$ diluted in $[Co(NO)Br(diars)_2]^+$ at 300 K in the *bc* plane.

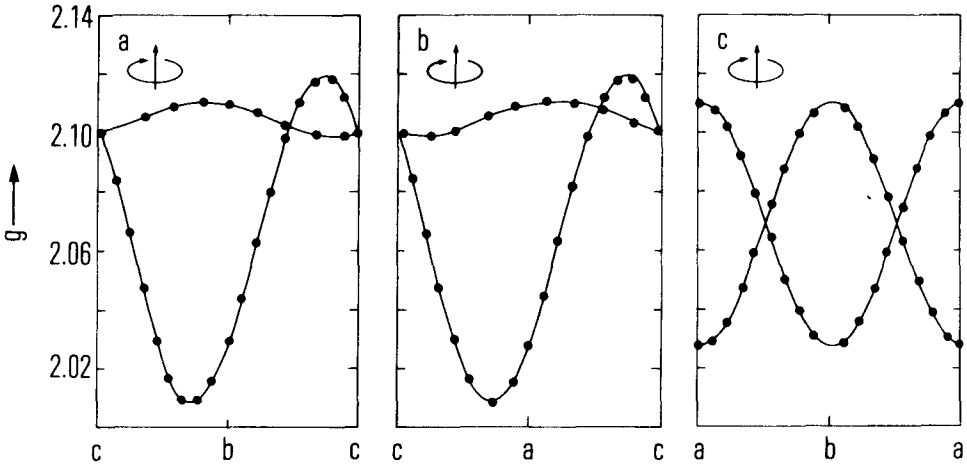

Figure 3. Experimental (● ● ●) and computed (——) angular variation of g from single crystal Q-band EPR spectra at 300 K in the three orthogonal planes.

detailed analysis. However, it has been found that all the four As atoms and two Br atoms contribute to the multiplet structure. Again because of considerable overlap due to spectra at different orientations we have chosen some of the unique orientations to identify the hyperfine splitting due to the ^{75}As and $^{79,81}Br$ nuclei. In view of the slight difference in the nuclear magnetic moments of ^{79}Br and ^{81}Br, very small separation of

Table 1. Principal values of g and ligand hfs tensors for $[NiBr_2(diars)_2]Br$ diluted in $[Co(NO)Br(diars)_2]Br$ single crystals.

		Direction cosines		
		a	*b*	*c*
Site 1	$g_{xx} = 2{\cdot}120$	−0·239	−0·396	0·887
	$g_{yy} = 2.110$	0·971	−0·125	0·205
	$g_{zz} = 2{\cdot}008$	0·030	0·910	0·414
Site 2	$g_{xx} = 2{\cdot}120$	0·396	−0·239	−0·887
	$g_{yy} = 2{\cdot}110$	0·125	0·971	−0·205
	$g_{zz} = 2{\cdot}008$	0·910	−0·030	0·41
	$A_{xx}(^{75}As) = -20\,G$		$A_{xx}(^{81}Br) = +52\,G$	
	$A_{yy}(^{75}As) = -25\,G$		$A_{yy}(^{81}Br) = -46\,G$	
	$A_{zz}(^{75}As) = -26\,G$		$A_{zz}(^{81}Br) = +130\,G$	
	$A_{av}(^{75}As) = -23{\cdot}7\,G$		$A_{av}(^{81}Br) = 45{\cdot}3\,G$	
	$A_{iso}(^{75}As) = 24{\cdot}7\,G$		$A_{iso}(^{81}Br) = 48{\cdot}5\,G$	

hyperfine lines due to them has been noticed and hence we report the values corresponding to ^{81}Br.

One of the most characteristic spectrum was obtained when the magnetic field was placed either in the 100 or 010 plane roughly 10° away from either the *b*- or *a*-axis respectively. The experimental spectrum measured along this direction is given in figure 2. The low-field lines correspond to nearly g_{xx} while the high-field multiplet corresponds to nearly g_{zz}. The simulated spectra corresponding to these g-values are given below and above the experimental spectrum respectively. Similar spectra with little change in the anisotropic values were obtained in another orientation corresponding to g_{yy} and g_{zz}. All the spin hamiltonian parameters for $NiBr_2(diars)_2^+$ are given in table 2 and compared with the other dihalo diphos and diars complexes of Ni(III).

It may be noted that hyperfine splitting constants due to ^{75}As is essentially isotropic and the A_{av} of 23·7 G obtained from the present single crystal EPR data compared very well with the A_{iso} of 24·7 G (Manoharan and Rogers 1970). In addition the anisotropic hyperfine splitting constants due to $^{79,\,81}Br$ have been given signs by comparison of the magnitudes of the principal values with that of the isotropic value obtained earlier. The principal values of $A(Br)$ are:

$$A_{xx} = +52\text{ G},$$

$$A_{yy} = -46\text{ G},$$

$$A_{zz} = +130\text{ G},$$

giving an A_{av} of 45·3 G which compares again well with the A_{iso} value of 48·5 G (Manoharan and Rogers 1970).

3.1d *Electronic structure of* $[NiBr_2(diars)_2]Br$: With the knowledge of the relative signs of the various hyperfine coupling constants, it would be possible to decipher the electronic structure of the complex ion $[NiBr_2(diars)_2]^+$ and compare it with other diphos and diars systems.

In earlier cases mentioned in §1, it has been proved that the unpaired electron in these

Table 2. Spin hamiltonian parameters of $NiX_2(L\text{-}L)_2^+$.

No.	$NiX_2(L\text{-}L)_2^+$	g-tensor values	A-tensor values in gauss		References
			A(L-L)	$A(X)$	
1.	$NiCl_2(diphos)_2^+$	$g_{xx} = 2{\cdot}119$	$A_{xx} = -13$ (1)	$A_{xx} = -15{\cdot}3$ (1)	Sethulakshmi *et al* (1979)
	L-L = P-P	$g_{yy} = 2{\cdot}113$	$A_{yy} = -5$ (1)	$A_{yy} = -18.3$ (1)	
	X = Cl	$g_{zz} = 2{\cdot}010$	$A_{zz} = -43{\cdot}6$ (1)	$A_{zz} = -17{\cdot}6$ (1)	
2.	$NiCl_2(diars)_2^+$	$g_{xx} = 2{\cdot}142$	$A_{xx} = -8{\cdot}5$	$A_{xx} = -32$	Bernstein and
	L-L = As-As	$g_{yy} = 2{\cdot}142$	$A_{yy} = -6{\cdot}1$	$A_{yy} = -50$	Gray (1972)
	X = Cl	$g_{zz} = 2{\cdot}008$	$A_{zz} = -32$	$A_{zz} = -29$	
3.	$NiBr_2(diphos)_2^+$	$g_{xx} = 2{\cdot}141$	$A_{xx} = -20$ (2)	$A_{xx} = -27$ (1)	Sethulakshmi *et al* (1979)
	L-L = P-P	$g_{yy} = 2{\cdot}096$	$A_{yy} = -20$ (2)	$A_{yy} = -61$ (1)	
	X = Br	$g_{zz} = 1{\cdot}994$	$A_{zz} = -19{\cdot}4$ (1)	$A_{zz} = -169$ (1)	
4.	$NiBr_2(diars)_2^+$	$g_{xx} = 2{\cdot}120$	$A_{xx} = -20$ (1)	$A_{xx} = +52$ (1)	Present work
	L-L = As-As	$g_{yy} = 2{\cdot}110$	$A_{yy} = -25$ (1)	$A_{yy} = -46$ (1)	
	X = Br	$g_{zz} = 2{\cdot}008$	$A_{zz} = -26$ (1)	$A_{zz} = +130$ (1)	

Ni(III) systems is in an essentially d_z^2 orbital. Assuming direct spin transfer into the orbitals of the axial Br atoms and the in-plane σ- and π-orbitals of As atoms, it is obvious that the A_{zz} of ^{79,81}Br and ^{75}As must be of opposite signs, the former being positive. The values assigned to the isotropic and the anisotropic hyperfine coupling constants can be used to calculate spin densities on the ligand nuclei and hence the molecular wave function containing the unpaired electron. The isotropic and dipolar coupling constants for the unpaired electron were taken from Ayscough (1967). The experimental spin densities are given in table 3.

The $NiBr_2As_4$ chromophore may be assigned a D_{2h} symmetry though the correct molecular symmetry in the host lattice could be lower. The only optical transition observed at 14,500 cm^{-1} for this complex in solution can be assigned to $^2A_g \rightarrow {}^2B_{2g}$ and $^2A_g \rightarrow {}^2B_{3g}$ which are nearly degenerate. Evaluating the g-values to first order by using the relation

$$g_\perp = 2.0023 - \frac{6\lambda}{\Delta},$$

where $\lambda = -272\ cm^{-1}$ for Ni(III), we find $g_\perp$ turns out to be 2·115 (observed values are $g_{xx} = 2{\cdot}120$ and $g_{yy} = 2{\cdot}110$) and $g_\parallel$ is found to be near to that of free spin. Though this excludes contribution from ligand spin-orbit coupling, a simple correlation of this kind indicates a d_{z^2} ground state and the correctness of the proposed excited states mentioned above.

The ground state for these ions $^2A_g(z^2)$ shall be derived from the electronic configuration

$$[a_g(x^2-y^2)]^2 < [b_{2g}(xz)]^2 < [b_{3g}(yz)]^2 < [a_g(z^2)]^1 < [b_{1g}(xy)]$$

with the only empty d-orbital being d_{xy}. The LCAO-MO for the unpaired electron can be written (Bernstein and Gray 1972) as

$$\begin{aligned} a_g(d_{z^2}) = {} & a_1 d_{z^2} + a_2\phi_{p_z}(\mathrm{Br}) + a_3\phi_s(\mathrm{As}) \\ & - a_4\phi_{p_\sigma}(\mathrm{As}) - a_5\phi_{p_z}(\mathrm{As}) - a_6\phi_s(\mathrm{Br}) - a_7\phi_{p_x}(\mathrm{Br}), \end{aligned} \tag{1}$$

where a_1 and a_2, a_3 etc are metal and ligand orbital coefficients respectively and the ϕ's are ligand orbital combinations, defined as*

$$\phi_{p_z}(\mathrm{Br}) = 1/\sqrt{2}[p_z(\mathrm{Br}_1) - p_z(\mathrm{Br}_2)]$$

Table 3. Spin densities from ligand hfs tensor for [NiBr(diars)$_2$]Br doped [Co(NO)Br(diars)$_2$]Br single crystals.

	A (gauss)	ρ(%)
^{75}As	$A_{iso} = -23{\cdot}67$	$\rho_{4s} = 0.69$
	$A_{dip\cdot major} = 4{\cdot}00$	$\rho_{4p\sigma} = 2{\cdot}19$
	$A_{dip.minor} = 0{\cdot}66$	$\rho_{4p\pi} = 0{\cdot}36$
	$A_{iso} = 45{\cdot}17$	$\rho_{4s} = 0{\cdot}54$
^{81}Br	$A_{dip.major} = 117{\cdot}67$	$\rho_{4p\sigma} = 20{\cdot}86$
	$A_{dip\cdot minor} = 52{\cdot}00$	$\rho_{4p\pi} = 9{\cdot}22$
		$\rho_{(As)} = 12{\cdot}96$
		$\rho_{(Br)} = 61{\cdot}24$
		$\rho_{(ligand)} = 74$

$$\phi_s(\text{As}) = (1/\sqrt{2})\,[s(\text{As}_1) + s(\text{As}_2) + s(\text{As}_3) + s(\text{As}_4)]$$

$$\phi_{p_\sigma}(\text{As}) = (1/2)\,[p_x(\text{As}_1) - p_x(\text{As}_2) + p_x(\text{As}_3) + p_x(\text{As}_4)]$$

$$\phi_{p_\pi}(\text{As}) = (1/2)\,[p_y(\text{As}_1) + p_y(\text{As}_2) - p_y(\text{As}_3) - p_y(\text{As}_4)]$$

$$\phi_s(\text{Br}) = (1/\sqrt{2})\,[s(\text{Br}_1) + s(\text{Br}_2)],$$

$$\phi_{p_x}(\text{Br}) = (1/\sqrt{2})\,[p_x(\text{Br}_1) - p_x(\text{Br}_2)].$$

The ligand orbital coefficients are directly obtained from the spin-density data given in table 3. The total unpaired electron density on the ligand turns out to be 74%. Imposing the normalization condition on equation (1), we get

$$\int |\psi(d_{z^2})|^2 \, d\tau = a_1^2 + \sum_{j=2}^{7} a_j^2 + 2a_1 \sum_{j=2}^{7} a_j S_{ij} = 1, \tag{3}$$

Where S_{ij}'s are the overlap integrals evaluated by using Richardson's functions (Richardson *et al* 1962) for the metal atom and Clementi's functions (Clementi 1965) for the ligands. Using equation (3) and a_j's we obtain the metal-orbital coefficient a_1. The overlap integrals and the MO coefficients are listed in table 4. Comparison of these coefficients with those for the other diars and diphos complexes of Ni(III) (table 5), gives an idea of the quantitative changes in the modes of bonding as we go from P to As in Group VB and from Cl to Br in group VII B.

The EPR results of $[NiBr_2(diars)_2]^+$ together with the results reported earlier show considerable delocalization of the unpaired spin density. Ligand hyperfine tensors and an approximate LCAO-MO approach show an increase of covalency in the order $[NiCl_2(diphos)_2]^+ < [NiCl_2(diars)_2]^+ < [NiBr_2(diars)_2]^+ < [NiBr_2(diphos)_2]^+$ in slight disagreement with our earlier predictions (Sethulakshmi *et al* 1979). It is worthwhile to mention here that some of the errors due to improper normalisation of the wavefunctions in the earlier works have now been corrected. A comparison indicates that the total unpaired spin density in the ligands increases in the same order

$$NiCl_2(diphos)_2^+ (68{\cdot}6\,\%) < NiCl_2(diars)_2^+ (76{\cdot}8\,\%),$$

$$< NiBr_2(diars)_2^+ (74\,\%) < NiBr_2(diphos)_2^+ (86{\cdot}1\,\%).$$

In the bromo complexes, there is considerable σ delocalization onto the axial bromines, leading to a net higher covalency. It is striking that the covalency increases whenever the

Table 4. Overlap integrals and molecular orbital coefficients for $[NiBr_2(diars)_2]Br$.

Atomic orbitals	a_j	Group overlap *integrals* S_{ij}
ϕ_{p_z}(Br)	0·45672	0·06713
s(As)	0·08307	0·09524
p_σ(As)	0.14799	0·12883
p_π(As)	0·06000	0
s(Br)	0·07349	0·04066
p_x(Br)	0·30365	0
d_{z^2}(Ni)	0·7969	—

Table 5. Molecular orbital coefficients and overlap integrals for a series of dihalo diphos and diars complexes of low-spin d^7 Ni(III).

	$[NiCl_2(diphos)_2]^+$ L = P X = Cl		$[NiBr_2(diphos)_2]^+$ L = P X = Br		$[NiCl_2(diars)_2]^+$ L = As X = Cl		$[NiBr_2(diars)_2]^+$ L = As X = Br	
A.O's	a_j	S_{ij}	a_j	S_{ij}	a_j	S_{ij}	a_j	S_{ij}
p_z(X)	0·1414	0·0742	0·4123	0·0671	0·3742	0·0742	0·4567	0·0671
s(L)	0·0775	0·1030	0·0775	0·1030	0·0678	0·0952	0·0831	0·0952
p_σ(L)	0·3507	0·1378	0·0227	0·1373	0·3017	0·1288	0·1480	0·1288
p_π(L)	0·1581	0	0·0227	0	0·0707	0	0·06	0
s(X)	0·1	0·0482	0·1	0·0407	0·1414	0·0482	0·0735	0·0407
p_x(X)	0·0707	0	0·2074	0	0·1483	0	0·3036	0
d_{z^2}(Ni)	0·9359	—	0·8495	—	0·8585	—	0·7969	—

4*s* and 4*p* orbitals are involved. This must be due to the extended radial part of the wave functions of 4*s* and 4*p* orbitals. In $[NiCl_2(diphos)_2]^+$, the unpaired electron is least delocalized onto the ligands in this series since both phosphorous and chlorine orbitals involved in the MO formation are of the 3*s* and 3*p* type.

3.2 EPR *of pure* $[NiBr_2(diars)_2]Br$

$[NiBr_2(diars)_2]Br$ is isomorphous to $[NiCl_2(diars)_2]Cl$ whose crystal structure is known (Berstein *et al* 1972). The crystal is monoclinic with two molecules per unit cell and the differences in their orientations are clear from figure 4 where the projection in the *ac** plane is shown.

3.2a *g-Tensor*: The principal *g*-values for $[NiBr_2(diars)_2]Br$ obtained by a diagonalisation procedure, agree very closely with the powder *g*-values reported by Manoharan and Rogers (1970). A single line was observed at all orientations at both *X*- and *Q*-band frequencies, which clearly indicates that there is exchange between the two sites and that it is stronger than one half of the separation between them even at *Q*-band. To confirm this, we have calculated the average *g*-tensor from the two molecular *g*-tensors by taking their relative orientations (Mooij *et al* 1976). The principal *g*-values thus calculated are in reasonable agreement with experimental values. The direction cosines, however, differ to a greater extent than experimental values. All the values are listed in table 6 for comparison.

The angular variation of *g* was simulated in the *ac** plane (where the two sites are

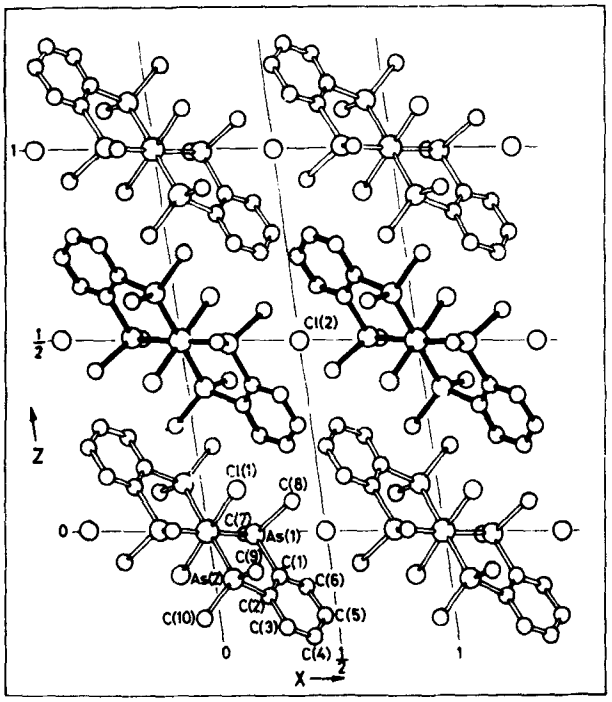

Figure 4. Projection of $NiCl_2(diars)_2^+$ on the *ac** plane (Bernstein *et al* 1972).

Table 6. Spin hamiltonian parameters[a] for $[NiBr_2(diars)_2]Br$.

g-tensor directions	Doped single crystal	Pure powder	Pure single crystal	Average g-tensor calculated
g_{xx}	2·120	2·119	2·119	2·120
g_{yy}	2·110	2·069	2·068	2·075
g_{zz}	2·008	2·043	2·043	2·044

	Direction cosines[b] for g_{av} (calculated)			Direction cosines[c] for pure crystal		
	a	*b*	*c**	*a*	*b*	*c**
g_{xx}	0·795	0	−0·606	0·702	0·185	−0·688
g_{yy}	0	1	0	0·283	0·920	0·273
g_{zz}	0·606	0	0·795	0·686	0·207	0·698

[a] g-value are accurate upto $\pm$ 0·001.
[b] Calculated using the direction cosines of the two sites obtained from the crystal structure.
[c] Obtained by the diagonalisation of the experimental values.

equivalent throughout and hence no effect of exchange is felt on the g-value) using the principal values from the doped case and the direction cosines from the crystal structure. The fit with the experimental variation is remarkable and is shown in figure 5a. This proves that the rhombic nature of the g-tensor arises not because of any change in the ground state but due to exchange averaging between magnetically inequivalent sites. Such an averaging of the g-tensor has been noticed in several other systems (Manoharan *et al* 1981; Ramakrishna and Manoharan 1984).

3.2b *Line width*: To get an idea of the variety of strength of the interactions, the line width was measured at X- and Q-band and frequencies in the *ab*, *bc* and *ac** planes. The understanding of the variation in the *ac** plane (where two sites are magnetically equivalent) is somewhat easier and hence is considered first.

The line shape analysis revealed that the line in *ac** plane is almost Lorentzian in character (figure 6) and this indicates that exchange is much stronger than any of the broadening mechanisms—dipolar or hyperfine.

A range of values of 700 G to 1000 G for the exchange parameter J_0, is obtained from the relation given by Van Vleck (1948) for strong exchange narrowing case

$$\Delta B_{pp} = \frac{2}{\sqrt{3}} \frac{M_2^{total}}{J_0} \tag{4}$$

where M_2 total is the total secular second moment from both the dipolar and hyperfine contributions and using ΔB_{pp} obtained from Q-band spectra.

The angular variation of the X- and Q-band line widths in the *ac** plane is shown in figure 5b. The fact that Q-band line widths are always smaller indicates that we are in a J-regime where secular and non-secular contributions to the line width are quite sensitive to the frequency of measurement with the non-secular parts becoming more pronounced at lower Zeeman frequencies.

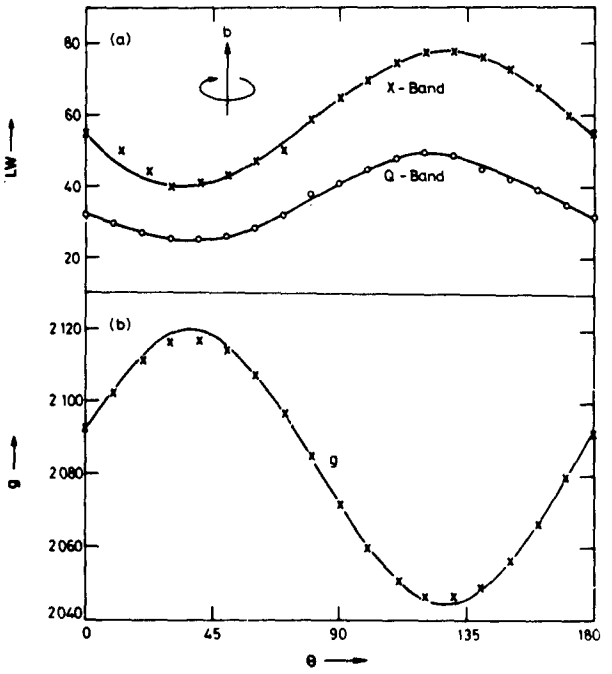

Figure 5. (**a**) Angular variation of line width in X- and Q-band spectra. (**b**) g-simulation for pure $[NiBr_2(diars)_2]Br$ in the ac^* plane at 300 K.

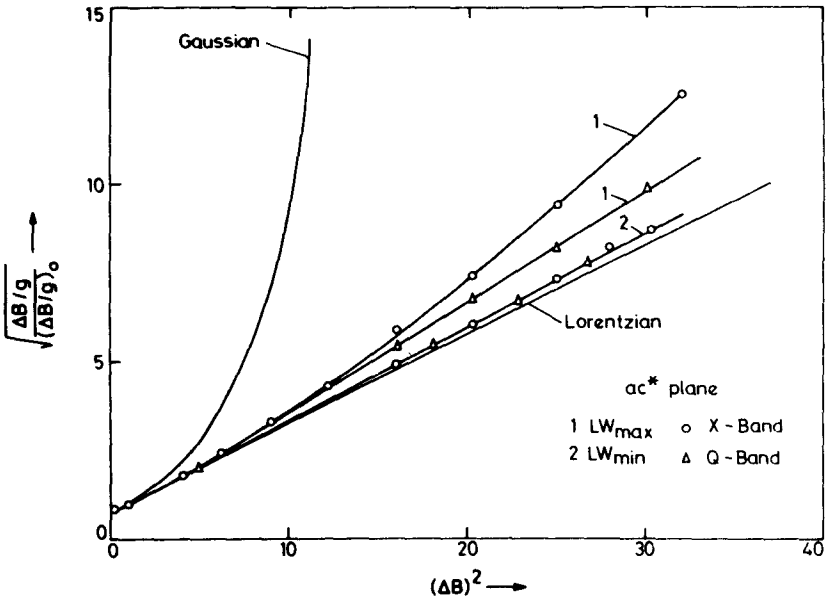

Figure 6. Line shape analysis for $[NiBr_2(diars)_2]Br$ at two arbitrary orientations of **B** in the ac^* plane.

Table 7. Local fields and $\Delta B_X - \Delta B_Q$ for $[NiBr_2(diars)_2]Br$ in ac^* plane from single crystal EPR results at 300 K.

Angle (°) of B_0 with a-axis	Dipolar[a] Second moments × 10^{-3} G²			Hyperfine[b] Second moments × 10^{-3} G²		$\Delta B_X - \Delta B_Q$ (gauss)
	$\Delta m = 0$	$\Delta m = \pm 1$	$\Delta m = \pm 2$	Secular	Non-secular	
40	1·55	6·05	1·94	6·90	14·60	28
60	1·86	5·72	1·91	10·52	13·73	27
80	2·79	4·54	1·95	18·19	11·87	24
100	2·49	4·63	1·89	26·06	9·92	21
120	1·51	5·51	1·79	30·63	8·79	17

[a] In calculating dipolar interaction the point-dipole has been resorted to.
A 5–10% increase is expected if the spin-delocalization is taken into account.
[b] Axially symmetry g- and A-tensors were assumed.
A-tensor values used are: $A_{\|}(As) = 26$ G $A_{\|}(Br) = 130$ G $A_{\perp}(As) = 22$ G $A_{\perp}(Br) = 50$ G.

We have used the method of Soos *et al* (1973) to obtain the fourier components of the spin correlation functions from the angular and frequency variation of line width for $kT \gg J$ with the knowledge of local fields. The method is useful when the sites become magnetically equivalent (which is true for $NiBr_2(diars)_2^+$ in the ac^* plane) and provides a direct test for the various theoretical models (Blume and Hubbard 1970; Anderson and Weiss 1953) of spin correlation functions. The angular dependence of the local field amplitudes computed *via* the second moments along with the experimental ΔB_X-ΔB_Q values at X- and Q-bands are summarised in table 7.

The total ΔB_{pp} is given by

$$\frac{\sqrt{3}}{2}\Delta B_{pp} = \Gamma_{total}$$
$$= \Gamma_{dipolar} + \Gamma_{hyperfine}$$
$$= M_2^{(0)} f(0) + M_2^{(1)} f(\omega_0) + M_2^{(2)} f(2\omega_0) + a^{(0)} g(0) + a^{(1)} g(\omega_0) \qquad (5)$$

where $g(\omega)$ is the fourier component of the autocorrelation function $C(t)$, and $f(\omega)$ is the Fourier component of $C^2(t)$. The Fourier components describe the time evolution due solely to the exchange hamiltonian and are independent of orientation in the strong coupling limit. Thus the angular variation of linewidth provides enough equations to evaluate all the five unknowns.

3.2c *Nonsecular spin correlations*: The nonsecular ($\omega \neq 0$) correlations have been calculated as was done by Soos *et al* (1973) by relating the difference between the X- and Q-band linewidths. The equations for various orientations are

$$\frac{\sqrt{3}}{2}[\Delta B_X(\theta, \phi) - \Delta B_Q(\theta, \phi)] = M_2^{(1)}(\theta, \phi)\Delta f(\omega)$$
$$+ M_2^{(2)}(\theta, \phi)\Delta f(2\omega) + a^{(1)}\Delta g(\omega), \qquad (6)$$

where $M_2^{(1)}$ and $M_2^{(2)}$ are the nonsecular dipolar second moments corresponding to $\Delta m = \pm 1$ and ± 2 respectively while $\Delta f(\omega)$ is the difference in the X- and Q-band Fourier

components at Larmor frequency, $\Delta f(2\omega)$ is the difference at twice the Larmor frequency and $\Delta g(\omega)$ is the corresponding difference for the hyperfine fourier component. By solving (6) by least squares procedure we have obtained

$$g(\omega) = 0{\cdot}152 \times 10^{-3}\mathrm{G}^{-1},$$
$$f(\omega) = 2{\cdot}68 \times 10^{-3}\mathrm{G}^{-1},$$
$$f(2\omega) = 1{\cdot}25 \times 10^{-3}\mathrm{G}^{-1}.$$

Using the *B–H* and *A–W* form for $C(t)$, the calculated values of the Fourier components were found to be smaller than the above mentioned experimental ones. This coupled with the fact that the angular dependence of the '10/3 effect' is not very well reproduced by the above fourier components suggests that we are in a regime where the approximations involved in the above theories are not quite valid. Also very different spin correlation functions may contribute to different orientations of the Zeeman field.

3.2d *Secular spin correlations*: Using the nonsecular Fourier components obtained, we tried to evaluate $g(0)$ and $f(0)$ by fitting the total linewidth. Unique positive values for either $g(0)$ or $f(0)$ could not be obtained by solving (5) which clearly shows that these secular Fourier components are sensitive to orientation of the magnetic field **B**.

3.2e *Ratio method*: We have tried a more qualitative type of analysis which just uses the Kubo-Tomita (1954) theory to evaluate the exchange field by the ratio of the line width at two observation frequencies. The linewidth at any Zeeman frequency assuming a Gaussian correlation function is given by

$$\Delta\omega_{1/2} = (\pi/2)^{1/2}\left[\frac{M_2^{(0)}}{\omega_{e0}} + \frac{M_2^{(1)}}{\omega_{e1}}\exp\left(-\frac{\omega_{zee}^2}{2\omega_{e1}^2}\right) + \frac{M_2^{(2)}}{\omega_{e2}}\exp\left(-\frac{2\omega_{zee}^2}{\omega_{e2}^2}\right)\right], \qquad (7)$$

where $M_2^{(0)}$ is the secular ($\Delta m = 0$) dipolar second moment and $\omega_{er}(r = 0, 1, 2)$ are the exchange parameters for the different contributions, all taken to be equal to ω_0 in the large exchange limit. From the linewidth studies at two observation frequencies at *X*- and *Q*-bands, the ratio $\Delta B_X/\Delta B_Q$ can be measured and using $M_2^{(r)}$ from crystal structure, one can evaluate ω_0.

Assuming $\omega_{e0} = \omega_{el} = \omega_{e2} = \omega_e$, the ratios obtained at five orientations were used to evaluate the exchange parameter. The ratio at two Zeeman frequencies can be fitted to two values of exchange and a plot of the ratio $\Delta B_X/\Delta B_Q$ as a function of frequency for a particular orientation in ac^* plane is shown in figure 7. Only one value of the exchange frequency which is physically meaningful is chosen. Pleau and Kokoszka (1973) used the method of ratios effectively and the frequency obtained can be related to J in the high temperature approximation by an equation of Moriya (1956).

$$\hbar^2\omega_e^2 = \frac{8}{3}J^2 zS(S+1), \qquad (8)$$

where z is the number of neighbouring spins in the lattice. The ω_e value for $[NiBr_2(diars)_2]Br$ is obtained to be 2500 G and this yields a J value of 625 G which agrees well with earlier calculations.

3.2f *Intersite exchange.* The very fact that there is a single exchange averaged line at all orientations even at *Q*-band frequencies yields a lower limit for the intersite exchange parameter, J' of 200 G (which is half the maximum separation at *Q*-band in

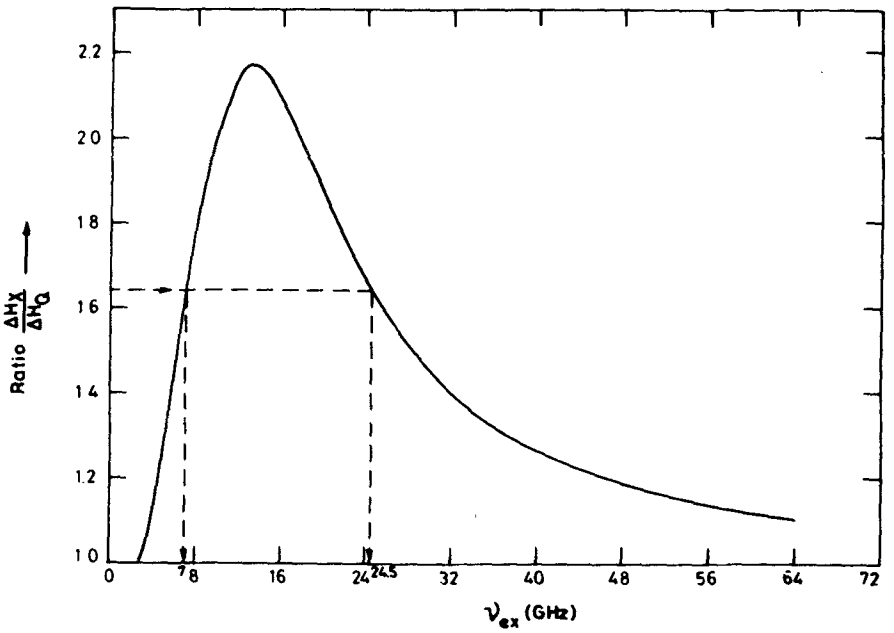

Figure 7. $\Delta B_X/\Delta B_Q$ ratio plotted against frequency for an arbitrary orientations in the ac^* plane.

the bc^* plane without any exchange). The angular variation of g for the two sites in the ab plane (without exchange) is shown in figure 8a. The intersite exchange parameter J' can be evaluated by the ΔB_{pp} variation in a plane where the two sites are magnetically inequivalent by measuring at X- and Q-band frequencies. The lines in the ab plane were nearly Lorentzian both in X- and in Q-band frequencies and hence the strong exchange limit is also applicable here.

Theories of exchange narrowing predict that the frequency dependent line width due to inequivalent sites (Yokota and Koide 1954; Hughes *et al* 1975) depends on the square of the splitting, ΔB_Q or ΔB_X, which ought to have been but for exchange,

$$\Delta B_{pp}(Q) - \Delta B_{pp}(X) = \frac{\Delta B_Q^2 - \Delta B_X^2}{B_e}, \tag{9}$$

where B_e is given by

$$(g\beta/h)B_e = 4t_c^{-1}(\sqrt{3}/2), \tag{10}$$

which t_c is a correlation time given by Hughes *et al* (1975) as

$$t_c = 0{\cdot}16\ \mathrm{h}\,|J|^{1/3}/|J'|^{4/3}. \tag{11}$$

The quantity B_e depends on the rate of exchange between the inequivalent sites. For large values of exchange, the Q-band line widths are always larger than the X-band line widths because the secular and nonsecular Fourier components are not frequency-dependent. But in this case as the value of exchange is rather small, the Q-band line width is smaller than the X-band line width at certain orientations are revealed by

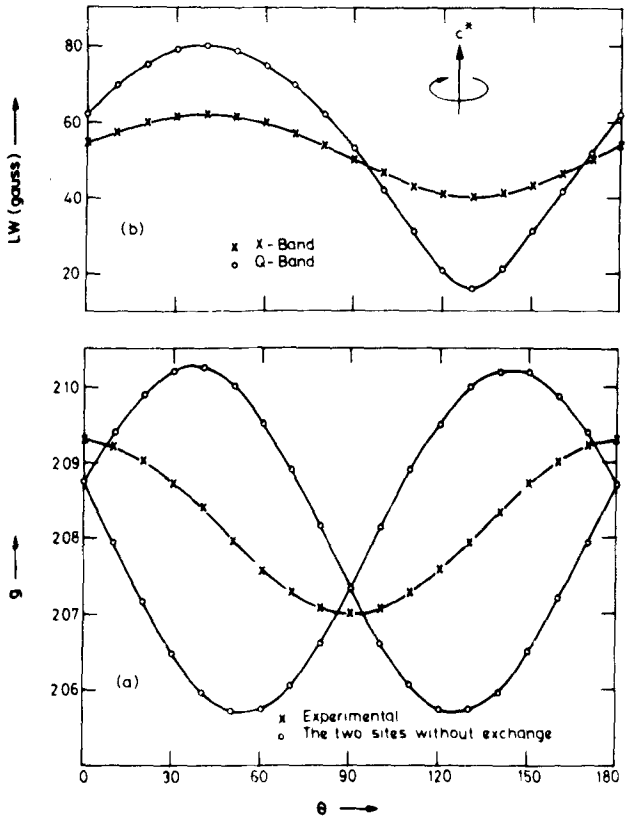

Figure 8. (**a**) Angular variation of g of the two sites in the *ab* plane without exchange (O O O) together with the observed g-variation of the single exchange narrowed line (× × ×). (**b**) The angular variation of line width in the *ab* plane at X-band (× × ×) and Q-band (O O O) at 300 K.

figure 8b. The value of B_e has been obtained to be 2000 G from the angular variation of the line width even though only one angle is sufficient.

The intersite exchange parameter J' was found to be 380 G assuming a value of 800 G for J. This shows that J' is of the same order as J and hence that $[NiBr_2(diars)_2]Br$ like its chloro analogue (Ramakrishna and Manoharan 1984) is close to a 3-d system. However, one cannot take the actual value of J' too literally as the formalism used above to calculate its value involves certain assumptions (Hughes *et al* 1975) which are not quite applicable to $[NiBr_2(diars)_2]Br$. Also such a small ratio of intrasite to intersite coupling makes the strong decoupling approximation used earlier for the dipolar four-spin correlation suspect.

4. Conclusion

The EPR spectra of $[NiBr_2(diars)_2)^+Br^-$ diluted in the tetragonal host lattice $[Co(NO)Br(diars)_2]^+Br^-$ show that there are two magnetically inequivalent sites with a very large bromine hyperfine splitting. The experimental g ligand hyperfine splittings

due to arsenic and bromine and spin densities are compared with other analogous diphos and diars complexes. The unpaired electron is essentially in the d_{z^2} orbital and there is extensive delocalization over all the ligand nuclei due to the extended 4*s* and 4*p* rae ial wavefunctions.

Also, the EPR study of pure, paramagnetic complex $[NiBr_2(diars)_2]Br$ indicates an averaging of the *g*-tensor due to weak exchange (800 G) and hence only a single line at all orientations at both *X*- and *Q*-band frequencies. This exchange averaging is the cause for the *g*-tensor variation with concentration. The basically Lorentzian line shape atleast near the centre implies that the value of exchange is much larger than the broadening mechanisms.

Neither the A–W model nor the B–H model could predict the Fourier components of the spin correlation function accurately and the values obtained were consistently lower than the ones determined by the study of the angular variation of the '10/3 effect'. The more qualitative Van Vleck procedure yields a value of 800 G for the exchange parameter and this agrees reasonably with the ratio method using the Kubo-Tomita model and Gaussian correlation function. We have estimated the intersite coupling to be 380 G which indicates that $[NiBr_2(diars)_2]Br$ is close to a 3-d system.

Acknowledgement

Grateful acknowledgement is due to the Department of Science and Technology, New Delhi for supporting this work. One of us (EBS) thanks VOC, Tuticorin and the UGC for a scholarship.

References

Anderson P W and Weiss P R 1953 *Rev. Mod. Phys.* **25** 269
Ayscough P B 1967 *Electron spin resonance in chemistry* (London: Methun)
Balasivasubramanian E, Sethulakshmi C N and Manoharan P T 1982 *Inorg. Chem.* **21** 1684
Bernstein P K and Gray H B 1972 *Inorg. Chem.* **11** 3035
Bernstein P K, Rodley G A, Marsh R and Gray H B 1972 *Inorg. Chem.* **11** 3040
Blume M and Hubbard J 1970 *Phys. Rev.* **B1** 3815
Clementi E 1965 *Tables of atomic functions* (I.B.M.)
Feltham R D and Nyholm R S 1965 *Inorg. Chem.* **4** 1334
Hughes R C, Morosin B, Richards P M and Duffy Jr W 1975 *Phys. Rev.* **1311** 1795
Kreisman P, Marsh R, Preer J R and Gray H B 1968 *J. Am. Chem. Soc.* **90** 1067
Kubo R and Tomita K 1954 *J. Phys. Soc. Jpn* **9** 888
Manoharan P T, Noordik J H, de Boer E and Keijzers C P 1981 *J. Chem. Phys.* **74** 1980
Manoharan P T and Rogers M T 1970 *J. Chem. Phys.* **53** 1682
Mooij J J, Klassen A A K and de Boer E 1976 *Mol. Phys.* **32** 879
Moriya T 1956 *Prog. Theor. Phys.* **16** 23
Nyholm R S 1950 *J. Chem. Soc.* 2061
Pleau E and Kokoszka 1973 *J. Chem. Soc. Faraday* **69** 355
Ramakrishna B L and Manoharan P T 1984 *Mol. Phys.* **52** 65
Richardson J W, Nieuport W C, Pavel R R and Edgell W F 1962 *J. Chem. Phys.* **36** 1057
Sethulakshmi C N, Subramanian S, Bennett M A and Manoharan P T 1979 *Inorg. Chem.* **18** 2520
Silverthorn W and Feltham R D 1967 *Inorg. Chem.* **6** 1662
Soos Z G, Huang T Z, Valentine J S and Hughes R C 1973 *Phys. Rev.* **B8** 993
Van Vleck J H 1948 *Phys. Rev.* **74** 1168
Yokota M and Koide S 1954 *J. Phys. Soc. Jpn* **9** 953